Astrophysical and Nuclear Physics Aspects of the r-Process

F.-K. Thielemann [a], C. Freiburghaus[a], T. Rauscher
Departement für Physik und Astronomie, Universität Basel, CH-4056 Basel, Switzerland

K.-L. Kratz, B. Pfeiffer
Institut für Kernchemie, Universität Mainz, D-55128 Mainz, Germany

J.J. Cowan[a]
Department of Physics and Astronomy, University of Oklahoma, Norman, OK 73019, USA

The formation of elements as heavy as Th and U and beyond is due to the rapid neutron-capture process (r-process), which causes the production of highly unstable nuclei near the neutron drip-line and functions via neutron captures, (γ,n)-photodisintegrations, β^--decays and beta-delayed processes. Neutrino-induced reactions may also play a possible role. Observations of abundances in old (low metallicity) stars indicate that it operates very early in galactic evolution, and is thus related to massive star progenitors forming supernovae and/or neutron stars. The abundances, being in all individual observations identical to solar r-abundances (at least for A>130), indicate a unique process and witness the interplay between nuclear structure far from beta-stability and the appropriate astrophysical environment. In previous studies we pursued a model-independent approach for the r-process as a function of neutron number densities n_n, temperatures T, and durations times τ. The present study follows the expansion of matter with an initial entropy S and an expansion timescales τ (more suited for astrophysical environments), which can also follow the freeze-out of reactions with declining temperatures and densities explicitely. We compare the similarities and differences between the two approaches. Special emphasis is given to constraints on nuclear properties far from stability, resulting from a comparison with solar r-process abundances in either approach. In particular the behavior of shell closures is examined. In addition, investigations are presented to test whether some features can also provide clear constraints on the permitted astrophysical conditions. We discuss supernova and neutron star merger scenarios with respect to these findings.

1 Introduction

The operation of an r-process is characterized by the fact that 10 to 150 neutrons per seed nucleus (in the Fe-peak or somewhat beyond) have to be available to form all heavier r-process nuclei by neutron capture. For a composition of Fe-group nuclei and free neutrons that translates into a neutron excess of $\eta=<(N\text{-}Z)/A>$=0.4-0.7 or an electron abundance, i.e. electron/nucleon or

[a]also participants of the Supernova Program, Institute for Theoretical Physics, University of California, Santa Barbara, CA 93106-4030

proton/nucleon ratio $Y_e = <Z/A> = 0.12$-0.3. Such a high neutron excess can only by obtained in a stellar environment through electron capture on protons or nuclei, which have to overcome large negative Q-values. This can be achieved by degenerate electrons with large Fermi energies and requires a compression to densities of $10^{11} - 10^{12}$g cm^{-3}, with a beta equilibrium between electron captures and β^--decays [4,32], as found in neutron star matter.

Another option is a so-called extremely alpha-rich freeze-out in complete Si-burning with moderate neutron excess $\eta<0.20$ and $Y_e>0.40$, respectively. After the freeze-out of charged particle reactions in matter which expands from high temperatures but relatively low densities, 70, 80, or 90% of all matter can be locked into ^{4}He with $N=Z$, which leaves even for moderate Y_e's a large neutron/seed ratio for the few existing heavier nuclei. The entropy per gram of baryons in a radiation dominated gas is proportional to T_9^3/ρ and can be used as a measure of the ratio between the remaining He mass-fraction and heavy nuclei, for a given Y_e and expansion timescale. Similarly, the ratio of neutrons to Fe-group (or heavier) nuclei (i.e. the neutron to seed ratio) is a function of entropy and permits for high entropies, with large remaining He and neutron abundances and small heavy seed abundances, neutron captures which proceed to form the heaviest r-process nuclei [62,37,52,63,22,23]. The behavior of these latter two environments is summarized in Fig. 1.

A different situation surfaces for maximum temperatures below freeze-out conditions for charged particle reactions with Fe-group nuclei. Then reactions among light nuclei which release neutrons, like (α,n) reactions on ^{13}C and ^{22}Ne, can sustain a neutron flux [53]. The constraint of having 10-150 neutrons per heavy nucleus, in order to attain r-process conditions, can only be met by small abundances of Fe-group nuclei. Such conditions were expected when a shock front passes the He-burning shell and enhances the ^{22}Ne(α,n) and ^{13}C(α,n) reactions by orders of magnitude. However, it could be shown that this neutron source is not strong enough for an r-process in realistic stellar models [2,8], i.e. would require unrealistically large amounts of such neutron sources. Recent research, based on additional neutron release via inelastic neutrino scattering [14], can also not produce neutron densities which are required for such a process to operate [61,34].

The r-process abundances $Y_{(Z,A)}$, measured in mole of nucleus (Z,A) per gram of matter, also witness the interplay between nuclear structure far from beta-stability and the appropriate astrophysical environment. Observations of heavy elements in low metallicity stars, with abundances of Fe/H being 1/1000 to 1/100 of solar, give information about stellar surface abundances, which are the abundances of the interstellar gas from which these stars formed early in galactic evolution. Such observations show on the one hand an apparently

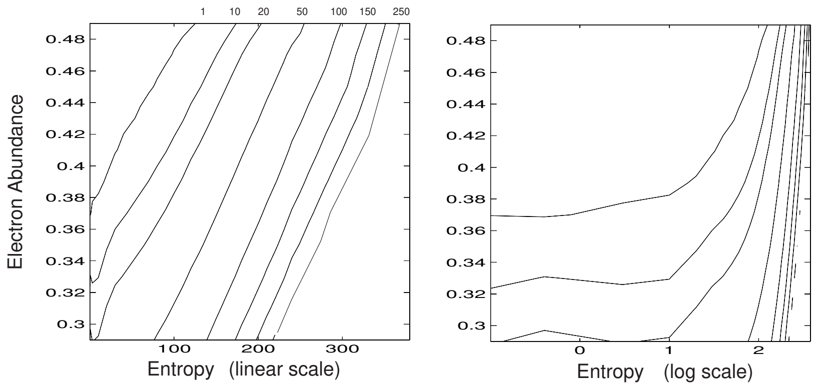

Figure 1: Y_n/Y_{seed} contour plots as a function of intial entropy S and Y_e for an expansion time scale of 0.05s, typical for type II supernova conditions. The left part shows how, for moderate Y_e-values, an increasing neutron/seed ratio, indicated by contour lines labeled with the respective Y_n/Y_{seed}, can be attained with increasing entropy, which leads to a stronger alph-rich freeze-out behavior. The results scale with Y_e, measuring the global neutron/nucleon ration 1-Y_e. The right part of the figure enhances on a logarithmic scale the low entropy behavior, where Y_n/Y_{seed} is only determined by the electron abundance Y_e. The contour lines are the same for both figures. A Y_n/Y_{seed} ratio of 150, which produces the heaviest r-process nuclei, would only be attained for a Y_e as small as 0.12.

completely solar r-process abundance pattern, at least for $A>130$, indicating that during such early times in galactic evolution only r-process sources and no s-process sources contributed to the production of heavy elements [49,9]. Fig. 2 shows a comparison (i) of solar r-abundances (summed up over isotopes to give element abundances), (ii) the observed abundances in the very low metallicity star CS-22892-052 [9], and (iii) the predictions by a theoretical model discussed in more detail in section 2.

On the other hand, it is also recognized that the r-process abundances come in with a delay of $>10^7$y after Fe and O [31], which excludes the higher mass SNe II as r-process sources, because such massive stars beyond 10-12$M_\odot$ have shorter evolution times. The r-process has generally been associated with the inner ejecta of type II supernovae [10,33], but also the decompression of neutron star matter (possibly in binary mergers) was suggested [30,32,13] and is consistent with the above mentioned low metallicity observations. Both these environments are complementary, either following low Y_e, low entropy conditions (decompression of neutron star matter) or a high entropy wind of the hot neutron star following type II supernova explosions [62,63,52].

Actual r-process calculations usually followed two different approaches.

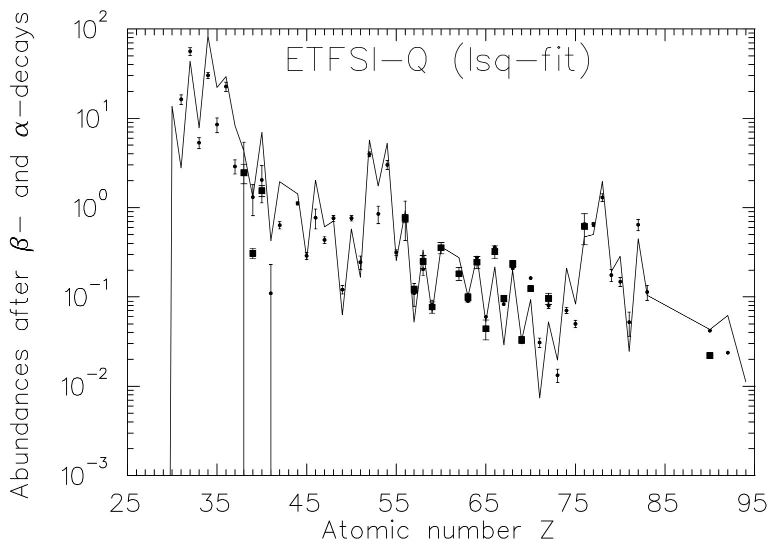

Figure 2: (i) Solar r-abundances for elements (scaled to 10^6 for solar Si) indicated by dots and error bars [25,59], (ii) observed abundances in the very low metallicity star CS-22892-052, given by filled squares and error bars [9] (being representative for all low metallicity stars and identical to solar r-abundances at least for $Z>56$), compared to (iii) theoretical predictions discussed in section 2 [43]. When using long-lived ^{232}Th, the star would have formed about 13-15 Gyrs ago, incorporating freshly synthesized r-process matter in the interstellar medium.

Some studies, focusing mostly on nuclear physics issues far from stability, made use of a model-independent approach for the r-process as a function of neutron number densities n_n and temperatures T, extending for a duration time τ [28,26,56,7,3,43,27]. Other studies usually stayed closer to a specific astrophysical environment and followed the expansion of matter on expansion timescales τ with an initial entropy S, passing through declining temperatures and densities until the freeze-out of all reactions [62,37,24,22,45,23,35,36,51]. Here we compare the similarities and differences between the two approaches and whether there actually exists a one-to-one relation. Special emphasis is given to constraints, resulting from a comparison with solar r-process abundances in either approach, on nuclear properties far from stability. In addition, investigations are presented to test whether some features can also provide clear constraints on the permitted astrophysical conditions. This relates mostly to the $A < 110$ mass range, where the high entropy scenario in supernovae faces problems.

2 Model-Independent Studies

The sequence of neutron captures, (γ, n)-photodisintegrations and beta-decays (and possibly additional reactions like beta-delayed neutron emission, fission etc.) have in principle to be followed with a detailed reaction network, given by a system of (several thousand) coupled differential equations with a dimension equal to the number of isotopes. This can be done efficiently [10], however, approximations are also applicable for neutron densities and temperatures well in excess of $n_n > 10^{20}\,\mathrm{cm}^{-3}$ and $T > 10^9\,\mathrm{K}$, which cause reaction timescales as short as $\approx 10^{-4}\,\mathrm{s}$ [5,3,19]. As the beta-decay half-lives are longer, roughly of the order of $10^{-1}\,\mathrm{s}$ to a few times $10^{-3}\,\mathrm{s}$, an equilibrium can set in for neutron captures and photodisintegrations. Such conditions allow to make use of the "waiting point approximation", sometimes also called the "canonical r-process", which is equivalent to an $(n,\gamma)-(\gamma,n)$-equilibrium $[n_n\langle\sigma v\rangle_{n,\gamma}^{Z,A}Y_{(Z,A)} = \rho N_A\langle\sigma v\rangle_{n,\gamma}^{Z,A}Y_nY_{(Z,A)} = \lambda_{\gamma,n}^{Z,A+1}Y_{(Z,A+1)}]$ for all nuclei in an isotopic chain with charge number Z. As the photodisintegration rate $\lambda_{\gamma,n}^{Z,A+1}$ is related to the capture rate $\langle\sigma v\rangle_{n,\gamma}^{Z,A}$ by detailed balance and proportional to the capture rate times $\exp(-Q/kT)$, the maximum abundance in each isotopic chain (where $Y_{(Z,A)} \approx Y_{(Z,A+1)}$) is located at the same neutron separation energy S_n, being the neutron-capture Q-value of nucleus (Z,A). This permits to express the location of the "r-process path", i.e. the contour lines of neutron separation energies corresponding to the maximum in all isotopic chains, in terms of the neutron number density n_n and the temperature T in an astrophysical environment, when smaller effects like ratios of partition functions are neglected [10].

The nuclei in such r-process paths, which are responsible for the solar r-process abundances, are highly neutron-rich, unstable, and located 15-35 units away from β-stability with neutron separation energies of the order S_n = 2-4 MeV. These are predominantly nuclei not accessible in laboratory experiments to date. Exceptions exist in the A = 80 and 130 peaks [28,26] and continuous efforts are underway to extend experimental information in these regions of the closed shells N=50 and 82 with radioactve ion beam facilities. The dependence on nuclear masses or mass model predictions enters via S_n. The beta-decay properties along contour lines of constant S_n towards heavy nuclei [56] (see Fig. 3 for the region around the N=82 shell closure) are responsible for the resulting abundance pattern. The build-up of heavy nuclei is governed within the waiting point approximation only by effective decay rates λ_β^Z of isotopic chains. Then the environment properties n_n and T (defining the S_n of the path), and the duration time τ, predict the abundances. In case the duration time τ is larger than the longest half-lives encountered in such a path, also a steady flow of beta-decays will follow, making the abundance ratios independent of τ ($\lambda_\beta^Z Y_{(Z)} = const.$ for all Z's, where $Y_{(Z)}$ is the total abundance of an isotopic chain and λ_β^Z its effective decay rate).

One has to recognize a number of idealizations in this picture. It assumes

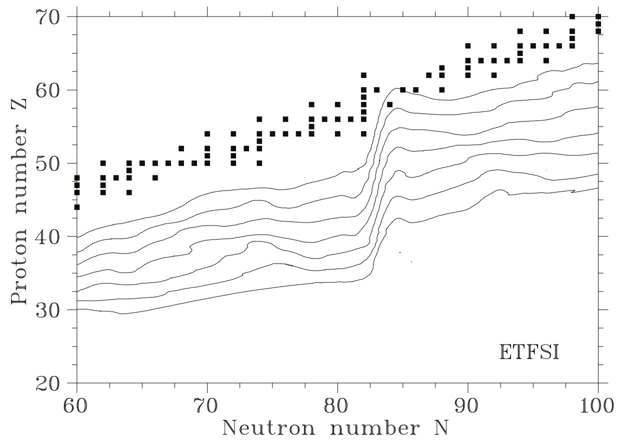

Figure 3: Contour plots of constant neutron separation energies S_n=1,2,3,4,5,6, and 7 MeV in the $80 \leq A \leq 140$ mass region for the ETFSI mass model[1]. The saddle point behavior before the shell closure at $N = 82$, also existing when using the FRDM masses[39], causes a deep trough before the peak at $A = 130$ (see upper part of Fig. 4), as the step from the abundance maximum of an isotopic chain Z to $Z + 1$ can also cause a large jump in N or equivalently A, leading to a large number of unpopulated mass numbers A.

a constant $S_n(n_n, T)$ over a duration time τ. Then the nuclei will still be existent in form of highly unstable isotopes, which have to decay back to beta-stability. In reality n_n and T will be time-dependent. As long as both are high enough to ensure the waiting point approximation, this is not a problem, because the system will immediately adjust to the new equilibrium and only the new $S_n(n_n, T)$ is important. The prominent question is whether the decrease from equilibrium conditions in n_n and T (neutron freeze-out), which initially ensure the waiting point approximation, down to conditions where the competition of neutron captures and beta-decays has to be taken into account explicitely, will affect the abundances strongly. In our earlier investigations we considered a sudden drop in n_n and T, leading to a sudden "freeze-out" of this abundance pattern, and only beta-decays and also beta-delayed properties [neutron emission and fission] have to be taken into account for the final decay back to stability[26].

When following this strategy, the analysis of the solar-system isotopic r-process abundance pattern showed that a minimum of three components with different S_n's, characterizing different r-process paths, was necessary for correctly reproducing the three peaks at $A \simeq 80$, 130, and 195 and the abundances in between[54,26]. The "low-A wings" of the peaks (when making use of exper-

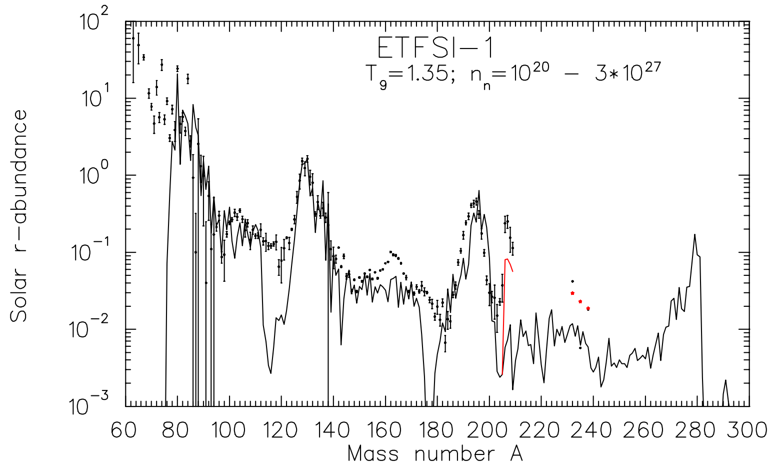

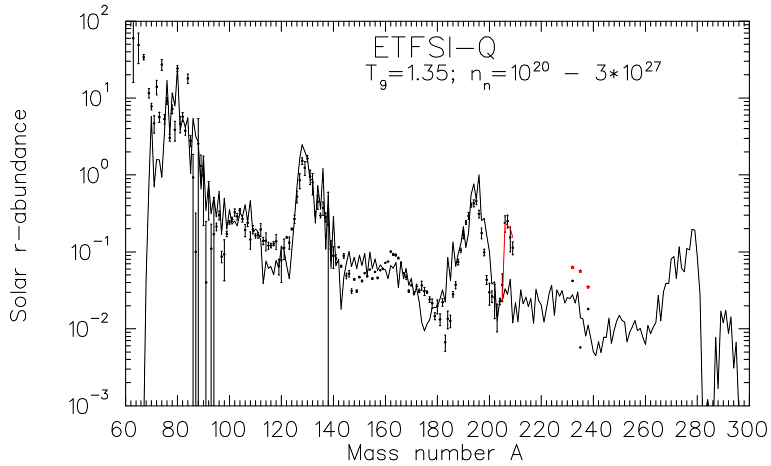

Figure 4: Fits to solar r-process abundances [25], obtained with 17 equidistant $S_n(n_n, T)$ components from 1 to 4 MeV. In the upper part, the result is presented for ETFSI masses with half-lives $\tau_{1/2}$ and beta-delayed neutron emission P_n values from QRPA calculations. In the lower part, the ETFSI-Q mass model [41] was applied, which introduced a phenomenological quenching of shell effects, comparable to HFB calculations with the Skyrme force SkP [12]. The quenching of the $N = 82$ shell gap leads to a filling of the abundance troughs and to a better overall reproduction of the heavy mass region. These results [43] are also the first ones which show a good fit to the r-process Pb and Bi contributions after following the decay chains of unstable heavier nuclei. For ^{232}Th and ^{235,238}U the solar and r-process production abundances are shown, allowing apparently for an increasing amount of decay with decreasing decay half-lives (in the sequence 232, 238, 235).

imental beta-decay properties at the magic neutron numbers $N = 50$ and 82), as well as the abundance pattern down to the next peak, could be reproduced, even with the assumption of a steady flow of beta-decays. This indicates that the astrophysical duration timescales τ are large in comparison to most of the beta-decay half-lives encountered and only comparable to the longest half-lives in the peaks (where the path comes closest to stability, see e.g. a 2 MeV contour line in Fig. 3), which control the leaking out to larger A's. A continuous superposition of components with varying n_n, T or $S_n(n_n, T)$ (rather than only three), as expected in an astrophysical environment, with equidistant steps in S_n between 2 and 4 MeV and τ between 1 and 2.5 s led to a slight, but not dramatic, change/improvement of the abundance curve [29].

When calculations [26] were supplemented by use of the most modern mass formula data [Finite Range Droplet Model FRDM [39] and Extended Thomas-Fermi model with Strutinski Integral ETFSIi [1], instead of using a somewhat dated but still very successful droplet model [20], we could show that abundance troughs appeared before (and after) the 130 and 195 abundances peaks, due to the behavior of the S_n contour lines of these mass models [56,7]. The location in N of an r-process path with a given S_n does not behave smoothly as a function of Z. Fig. 3 indicates a sudden jump to the position of the magic neutron number, where the contour lines show a saddle point behavior for the FRDM as well as ETFSI mass models. The population gap of nuclei as a function of A leads after decay to the abundance trough of Fig. 4. The upper part of Fig. 4 shows the abundance curve obtained with ETFSI nuclear masses [1] and beta-decay properties from a quasi-particle random-phase approximation QRPA [38]. When using FRDM masses [39] instead of the ETFSI predictions, a similar picture is obtained [56,3].

Additional tests were performed in order to see how this pattern could be avoided with different nuclear structure properties far from stability. The problem could be resolved [7], if for very neutron-rich nuclei the shell gap at the magic neutron number N=82 is less pronounced, i.e. quenched, than predicted by the global macroscopic-microscopic mass models. In light nuclei, the quenching of shells in neutron-rich isotopes is well established and a long-studied effect [40,6,17,50]. Hartree-Fock-Bogoliubov calculations [58,11,12] with a specific Skyrme force had exactly the expected effect on the r-process path and the resulting abundance curve [7]. This effect was recently also confirmed [41], when the ETFSI mass formula was phenomenologically quenched in a similar way as the HFB results and led to a very good agreement with solar r-abundances in a more systematic study [43] shown in the lower part of Fig. 4. An experimental investigation of shell quenching along the N=50 and 82 shell towards more neutron-rich nuclei (and approaching the r-process path for N=126) is a highly desirable goal in order to test the nuclear structure responsible for the solar abundances of heavy nuclei.

There are two aspects which have to be considered when trying to relate these simplified, model-independent results to astrophysics: (a) what kind of environments can produce the required conditions, and (b) do the nuclear structure conclusions drawn from the sudden freeze-out approximation stay valid for actual freeze-out timescales encountered in a specific environment? The second question cannot be answered in general, but only case by case. The question whether we understand fully all astrophysical sites leading to an r-process is not a settled one. There are strong indications that it is associated with type II supernovae. But galactic evolution timescales indicate that these can probably only be the low mass SNe II with longer evolution timescales [10,31], while neutron star mergers or still other sites are not necessarily excluded [30,32,13].

3 Parameter Studies for High Entropies

3.1 The Model and Nuclear Input

Recent r-process studies [63,52,45,23] have concentrated on the hot, neutron-rich environment in the innermost ejecta of type-II supernovae, also called the neutrino wind. These are the layers heated by neutrino emission and evaporating from the hot proto-neutron star after core collapse. These calculations obtain neutron separation energies of the r-process path S_n of $2-4\,\mathrm{MeV}$, in agreement with the conclusions of section 2. Whether the entropies required for these conditions can really be attained in supernova explosions has still to be verified. In relation to the questions discussed in section 2, it also has to be investigated whether a sudden freeze-out is a good approximation to these astrophysical conditions. In order to test this, and how explosion entropies can be translated into n_n and T (or S_n) of the model independent approach, we performed a parameter study based on the entropy S and the total proton to nucleon ratio Y_e (which measures the neutron-richness of the initial composition), in combination with an expansion timescale (for the radius of a blob of matter) of typically 0.05 s [52], and varied nuclear properties (i.e. mass models) like in section 2.

Thus, a hot blob of matter with entropy S, (i) initially consisting of neutrons, protons and some alpha-particles in a nuclear statistical equilibrium (NSE=complete thermal or chemical equilibrium ratios) given by Y_e, expands adiabatically and cools, (ii) the nucleons and alphas combine to heavier nuclei (typically Fe-group) with some neutrons and alphas remaining, (iii) for high entropies an alpha-rich freeze-out from charged-particle reactions occurs for declining temperatures, leading to nuclei in the mass range $A \approx 80-100$, and (iv) finally these remaining nuclei with total abundance Y_{seed} can capture the remaining neutrons Y_n and undergo an r-process. We chose a parameterized model for the expansion, essentially to introduce an expansion timescale, which makes these calculations independent of any specific supernova environment. But we will have to test later whether the expansion timescale employed is relevant to the supernova problem. The calculations were performed for a grid of entropies S and electron abundances Y_e ($S = 3, 10, 20, 30, \ldots 390 k_B$/baryon and $Y_e = 0.29, 0.31, \ldots 0.49$). Neutron capture rates were calculated with the new version of the statistical model code SMOKER [48]. The β^--rates came from experimental data or QRPA calculation [38].

Different mass zones have different initial entropies, which leads therefore to a superposition of different contributions in the total ejecta. For each pair of parameters Y_e and S, the calculations were initially started with a full charged particle nuclear network up to Pd. After the α-rich freeze-out, an r-process network, containing only neutron-induced reactions and beta-decay properties, followed the further evolution in a dynamical fashion [10,47]. The amount of subsequent r-processing depends on the available number of neutrons per heavy nucleus Y_n/Y_{seed} ($Y_{seed} = \sum_{A>4} Y_{(Z,A)}$). In Fig. 1a the Y_n/Y_{seed}-ratio is plotted in the (S, Y_e)-plane. A simple scaling with Y_e is clearly visible. Fig. 1b also shows that low Y_e-values would be one mean to avoid the very high entropies required to obtain large Y_n/Y_{seed}-ratios.

3.2 Superpositions of Entropies

The remaining question is, what kind of superposition of entropies the astrophysical environment provides. Earlier calculations [60] showed that the amount of mass ejected per entropy interval was relatively constant at late phases (when the higher entropy matter was expelled) and declining slightly at early phases (lower entropies) as a function of time (i.e. with increasing entropy). We did not perform complete hydro calculations, but rather followed these findings within a parametrized way, which allows to optimize for the best possible fit to the solar abundance distribution via a weighting function $g(S_i)$ with $g(S_i) = x_1 e^{-x_2 S_i}$, where i is the index of the components. We restrict ourselves here to two different Y_e-sequences with Y_e=0.45 and 0.49 shown in Fig. 5.

Entropies from about 200 to about 350 give Y_n/Y_{seed}-ratios growing from approximately 30 to 150. The α-rich freeze-out always produces seed nuclei in the range $90 < A < 120$. This material can then be "r-processed", leading to a fully neutron dominated process as discussed in section 2 and the components have a very similar abundance pattern in the mass range $A = 110-200$. Thus, it is possible for this entropy range to establish a one-to-one correspondence for abundances obtained in r-process conditions between entropy and expansion timescale (S, τ) in one type of calculation and a neutron separation energy of the r-path and timescale $(S_n(n_n, T), \tau)$ in the calculations discussed in section 2. The neutron separation energy S_n of the r-path is the one obtained during neutron capture freeze-out in the entropy based calculations. This correspondence can, however, only be established for entropies producing nuclei with $A>110$.

Matter for $A<110$ is a result of lower entropies with a neutron-poor and alpha-rich freeze-out, where the abundance of heavy nuclei is dominated by nuclei with alpha separation energies of ≈6 MeV and a specific $Z/A=Y_{e,heavy}$ of the dominating heavy nucleus after charged particle freeze-out, resulting from a given $Y_{e,global}$ [15,16]. None of the entropies produces an abundance peak at charged particle freeze-out with $A<80$, leaving a sufficient amount of neutrons for an r-processing which would reproduce the typical neutron-induced abundance features in the range $A=80-110$. A different choice of $Y_{e,global}$ (shown here for 0.45 and 0.49) can influence that pattern somewhat in avoiding very large spikes for $A\approx 90$ and $N=50$ isotopes, but the overall features stay.

Beyond $A=110$ different mass models (in Fig. 5 only ETFSI is shown) give fits of similar quality. The discrepancies below the $A=130$ r-process peak, in form of a pronounced trough, occur again for the FRDM and ETFSI mass model as in section 2. Thus, our results and conclusions from section 2 can be translated also to "realistic" astrophysical applications for this mass region. The nuclear structure properties leading to agreement and deficiencies apply in the same way, due to the nature of a fast freeze-out, which preserves the abundances as they result from an initial (n,γ)-(γ,n)-equilibrium at high temperatures, even when neutron captures and photodisintegrations are followed independently. Low entropies $(S=3-150)$ that contribute to the mass range between $90<A<140$ lead to an r-process with a fast (almost sudden) freeze out on short timescales of $\tau\approx 0.04\,\mathrm{s}$ [16]. Thus it is not surprising that the trough before $A=130$ (due to shell structure far from stability and its effect on abundance patterns in (n,γ)-(γ,n)-equilibrium) survives.

There is possibly one difference to the conclusions given with Fig. 4. The calculations experiencing the highest entropies have the longest neutron freeze-out timescales [16]. On the other hand, they are responsible for the heaviest nuclei with the largest neutron capture cross sections. Our results show that the trough before the $A=195$ peak, resulting in case of the ETFSI mass model and a waiting point approach, does not survive [56,7,3,43]. This r-process abundance region is changed by ongoing (non-equilibrium) captures during the

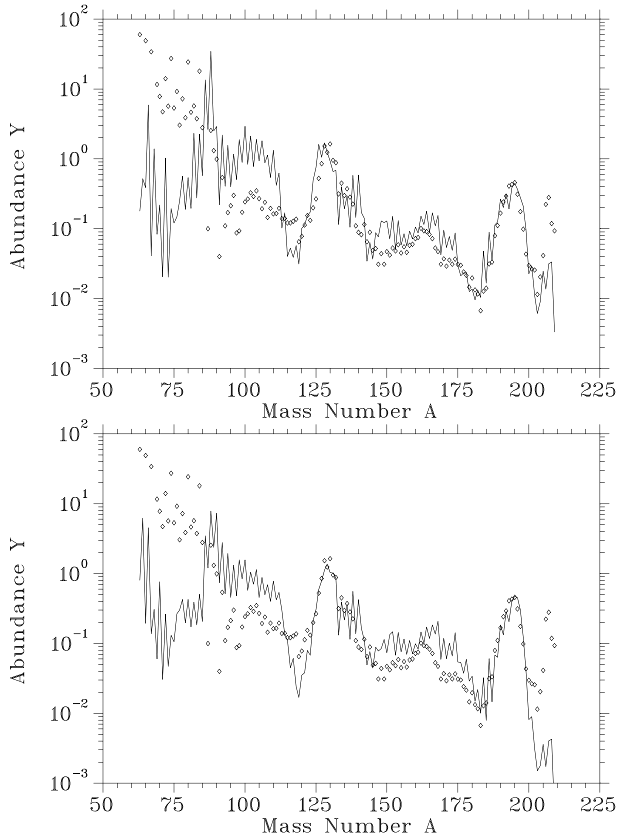

Figure 5: Similar to Fig. 4 with the ETFSI mass formula, making use of a superposition of entropies $g(S)$ to attain an overall good fit to solar r-process abundances from the high entropy neutrino wind in type II supernovae. These calculations were performed with $Y_e = 0.45$, and 0.49, but similar results are obtained in the range $0.30 - 0.49$, only requiring a scaling of entropy. The trough below $A = 130$ behaves similar to Fig. 4. This shows that a time dependent freeze-out (with a full treatment of neutron captures and photodisintegrations) resulting from a more realistic astrophysical scenario, can cause the same abundance deficiencies due to specific nuclear structure features as obtained in an instantaneous freeze-out from $(n,\gamma) - (\gamma,n)$-equilibrium. The trough before the $A = 195$ peak, existing e.g. for the ETFSI mass formula in the waiting point approximation and an instantaneous freeze-out, is filled due to non-equilibrium freeze-out neutron captures. The strong deficiencies in the abundance pattern below $A = 110$ are due to the alpha-rich freeze-out and thus related to the astrophysical scenario rather than to nuclear structure.

freeze-out and does not directly witness nuclear properties far from stability at the $N = 126$ shell closure. In Fig. 5 we actually observe a filling of the minimum before the $A = 195$ peak and even the ETFSI masses, that produced the largest trough in the waiting point calculations, seem to give a good fit.

There have been suggestions that neutrino-induced spallation of nuclei in the $A = 130$ peak, caused by the strong neutrino wind from the hot neutron star, could fill the abundance trough [46]. We refer to a more detailed discussion of this effect [55,15,16], including the requirements on neutrino luminosities and distances of matter from the neutron star at the time of the neutron freeze-out. We come to the conclusion that as an alternative interpretation the nuclear structure effects (shell quenching far from stability) outlined in detail in section 2 are still preferred, especially as they are already observed experimentally for lighter nuclei.

4 Conclusions

What can we learn from the entropy based studies and the fact that the r-process abundances below A=110 cannot be reproduced correctly? There are several possible conclusions: (a) the high entropy wind is not the correct r-process site (on the one hand due to the inherent deficiencies in the abundance pattern below $A = 110$ and the problems to obtain the high entropies in SNe II explosions, required for producing the massive r-process nuclei up to $A \simeq 195$ and beyond), or (b) the high entropy wind overcomes the problems to attain the high entropies and produces only the masses beyond $A = 110$, avoiding or diluting the ejection of the lower entropy matter. In the latter case another site is responsible for the lower mass region. An extension of Y_e to smaller values, as low as 0.3 for the $A<110$ mass region, could also solve the problem, and constraints on ν_e and $\bar{\nu}_e$ fluxes and mean energies in the supernova environment have been explored [45] to achieve this goal. But in addition to a lower Y_e, also lower entropies are required as they might come from cold high density matter in beta-equilibrium [16,4,32,21]. This can be deduced from Fig. 1b. It shows the Y_n/Y_{seed}-ratio plotted in the (S, Y_e)-plane with a logarithmic entropy axis and extends down to entropies as low as $S = 10^{-2}$, where a normal and not an alpha-rich freeze-out is encountered.

Whether such an interpretation ($A < 130$ from low Y_e and S conditions, $A > 130$ from high S conditions) is the solution, might eventually be answered by observations. There seems to exist meteoritic evidence [57], that the last r-process contributions to the solar system for A>130 and A<130 came at different times, i.e. from different types of events deduced from the extinct radioactivities ^{107}Pd, ^{129}I, and ^{182}Hf in meteoritic matter. It is highly desirable to have an independent verification of this from observations of low metallicity stars, which apparently show a completely solar r-process composition for nuclei with $A>130$ [49,9] (see Fig. 2), possibly stemming from the first events in our Galaxy which produce r-process nuclei[31]. It is also necessary to explore the abundances of nuclei with $A < 130$ in such observations, in order to test whether the solar pattern will also be found there or is absent, due to different evolution timescales of two independent stellar sources for these different mass ranges of r-process nuclei.

Acknowledgment

This work was supported by the Swiss Nationalfonds (grant 20-47252.96), the German BMBF (grant 06Mz864) and DFG (grant Kr80615), the US NSF (grant AST 9618332 and PHY 9407194) and the Austrian Academy of Sciencies.

References

1. Aboussir, Y., Pearson, J. M., Dutta, A. K., & Tondeur, F. 1995, At. Data Nucl. Data Tables, 61, 127
2. Blake, J.B., Woosley, S.E., Weaver, T.A., Schramm, D.N. 1981, Ap. J. 248, 315
3. Bouquelle, V., Cerf, N., Arnould, M., Tachibana, M., Goriely, S. 1996, A & A, 305, 1005
4. Cameron, A.G.W. 1989, in *Cosmic Abundances of Matter*, ed. C.J. Waddington, AIP Conf. Proc. 183, 349
5. Cameron, A.G.W., Cowan, J., Truran, J.W. 1983, Astopys. Space Sci., 91, 235
6. Campi, X., Flocard, H., Kerman, A.K., Koonin, S. 1975, Nucl. Phys. A, A251, 193
7. Chen, B., Dobaczewski, J., Kratz, K.-L., Langanke, K., Pfeiffer, B., Thielemann, F.-K., Vogel, P. 1995, Phys. Lett., B355, 37
8. Cowan, J.J., Cameron, A. G.W., Truran, J.W. 1983, Ap. J., 265, 429
9. Cowan, J.J., McWilliam, A., Sneden, C., Burris, D.L. 1997, Ap. J., 480, 246
10. Cowan, J. J., Thielemann, F.-K., Truran, J. W. 1991, Phy. Rep., 208, 267
11. Dobaczewski, J., Hamamoto, I., Nazarewicz, W., Sheikh, J. A. 1994, Phys. Rev. Lett., 72, 981
12. Dobaczewski, J., Nazarewicz, W., Werner, T. R. 1995, Phys. Scr., T56, 15

13. Eichler, D., Livio, M., Piran, T., Schramm, D. N. 1989, Nature, 340, 126
14. Epstein, R.I., Colgate, S.A., Haxton, W.C. 1988, Phys. Rev. Lett. 61, 2038
15. Freiburghaus, C., Kolbe, E., Rauscher, T., Thielemann, F.-K., Kratz, K.-L., Pfeiffer, B. 1997, Nucl. Phys. A621, 405c
16. Freiburghaus, C., Rembges, F., Rauscher, T., Kolbe, E., Thielemann, F.-K., Kratz, K.-L., Pfeiffer, B. 1997, Ap. J., submitted
17. Fukunishi, N., Otsuka, T., & Sebe, T. 1992, Phys. Lett., B296, 279
18. Goriely, S. 1996, Nucl. Phys. A605, 28
19. Goriely, S., Arnould, M. 1996, A & A, 312, 327
20. Hilf, E. R., von Groote, H., & Takahashi, K. 1976, in Proceedings of the 3rd International Conference on Nuclei far from Stability, Geneva, CERN-Rep 76-13, p.142
21. Hillebrandt, W., Takahashi, K., and Kodama, T. 1976, A & A 52, 63
22. Hoffman, R. D., Woosley, S. E., Fuller, G. M., Meyer, B. S. 1996, Ap. J., 460, 478
23. Hoffman, R. D., Woosley, S. E., Qian, Y.-Z. 1997, ApJ, 482, 951
24. Howard, W. M., Goriely, S., Rayet, M., & Arnould, M. 1993, Ap. J., 417, 713
25. Käppeler, F., Beer, H., Wisshak, K. 1989, Rep. Prog. Phys. 52, 945
26. Kratz, K.-L., Bitouzet, J.-P., Thielemann, F.-K., Möller, P., Pfeiffer, B. 1993, Ap. J. 402, 216
27. Kratz, K.-L., Pfeiffer, B., Thielemann, F.-K., 1997, Nucl. Phys. A, in press
28. Kratz, K.-L., Thielemann, F.-K., Hillebrandt, W., Möller, P., Harms, V., Truran, J. W. 1988, J. Phys. G, 14, 331
29. Kratz, K.-L., Thielemann, F.-K., Möller, P., Pfeiffer, B. 1994, in Proc. 8th Int. Symp. on Capture Gamma-Ray Spectroscopy, ed. J. Kern, IOP Bristol, p.724
30. Lattimer, J. M., Mackie, F., Ravenhall, D. G., Schramm, D. N. 1977, Ap. J., 213, 225
31. Mathews, G.J., Bazan, G., Cowan, J.J. 1992, Ap. J. 391, 719
32. Meyer, B. S. 1989, Ap. J., 343, 254
33. Meyer, B. S. 1994, Ann. Rev. Astron. Astrophys, 32, 153
34. Meyer, B.S., 1995, Ap. J. 449, L55
35. Meyer, B. S., Brown, J. S. 1997, Nucl. Phys. A621, 409c
36. Meyer, B. S., Brown, J. S. 1997, Ap. J. Suppl. 112, 119
37. Meyer, B.S., Mathews, G.J., Howard, W.M., Woosley, S.E., Hoffman, R.D. 1992, Ap. J 399, 656

38. Möller, P., Nix, J.R., Kratz, K.-L. 1997, At. Data Nucl. Data Tables 66, 131
39. Möller, P., Nix, J.R., Myers, W.D., Swiatecki, W.J. 1995, At. Data Nucl. Data Tables 59, 185
40. Orr, N. A. 1991, Phys. Lett. B258, 29
41. Pearson, J. M., Nayak, R. C., Goriely, S. 1996, Phys. Lett. B387, 455
42. Pfeiffer, B., Kratz, K.-L. 1996, KCh Mainz Report, unpublished
43. Pfeiffer, B., Kratz, K.-L., Thielemann, F.-K. 1997, Z. f. Phys. A357, 235
44. Qian, Y.-Z., Vogel, P., Wasserburg, G.J. 1997, Ap. J., submitted
45. Qian, Y.-Z., Woosley, S. E. 1996, Ap. J., 471, 331
46. Qian, Y.-Z., Haxton, W.C., Langanke, K., Vogel, P. 1996, Phys. Rev. C55, 1532
47. Rauscher, T., Applegate, J.H., Cowan, J.J., Thielemann, F.-K., Wiescher, M. 1994, Ap. J., 429, 499
48. Rauscher, T., Thielemann, F.-K., Kratz, K.-L. 1997, Phys. Rev. C56, 1613
49. Sneden, C., McWilliam, A., Preston, G. W., Cowan, J. J., Burris, D. I., Armosky, B. J. 1996, Ap. J. 467, 819
50. Sorlin, O. et al. 1993, Phys. Rev. C47, 2941
51. Surman, R., Engel, J., Bennett, J. R., Meyer, B. S. 1997, Phys. Rev. Lett. 79, 1809
52. Takahashi, K., Witti, J., Janka, H.-T. 1994, A&A, 286, 857
53. Thielemann, F.-K., Arnould, M., Hillebrandt, W. 1979, A & A, 74, 175
54. Thielemann, F.-K., Bitouzet, J.-P., Kratz, K.-L., Möller, P., Cowan, J. J., Truran, J. W. 1993, Phys. Rep., 227, 269
55. Thielemann, F.-K., et al. 1997, in *Capture Gamma-Ray Spectroscopy*, ed. G. Molnar, Springer Hungarica, in press
56. Thielemann, F.-K., Kratz, K.-L., Pfeiffer, B., Rauscher, T., van Wormer, L., & Wiescher, M. C. 1994, Nucl. Phys. A570, 329c
57. Wasserburg, G., Busso, M., Gallino, R. 1996, Ap. J. 466, L109
58. Werner, T. R., Sheikh, J. A., Nazarewicz, W., Strayer, M. R., Umar, A. S., Misu, M. 1994, Phys. Lett. B333, 303
59. Wisshak, K., Voss, F., Käppeler, F., Kerzakov, I. 1997, Nucl. Phys. A621, 270c
60. Witti, J., Janka, H.-T., Takahashi, K. 1994, A&A, 286, 841
61. Woosley, S.E., Hartmann, D., Hoffman, R.D., Haxton, W.C. 1990, Ap. J. 356, 272
62. Woosley, S. E., Hoffman, R. D. 1992, Ap. J. 395, 202
63. Woosley, S. E., Wilson, J. R., Mathews, G. J., Hoffman, R. D., Meyer, B. S. 1994, Ap. J. 433, 229